Mimicking Red Blood Cell Lipid Membrane To Enhance the Hemocompatibility of Large-Pore Mesoporous Silica

Robert A. Roggers, Madhura Joglekar, Justin S. Valenstein, and Brian G. Trewyn*,[†]

Department of Chemistry, Iowa State University, Ames, Iowa 50011-3111, United States

S *Supporting Information*

ABSTRACT: Mesoporous silica nanoparticles (MSNs) have been repeatedly demonstrated as potential drug-delivery devices. The study of biocompatibility and interaction of these materials with the various cell types is of great interest with regard to the development of viable pharmaceutical products. By mimicking the cholesterol, phosphatidylcholine, and phosphatidylethanolamine composition of the outer leaflet of a human red blood cell (RBC), lipid-bilayer-coated mesoporous silica particles show considerably improved hemocompatibility over phosphatidylcholine-coated and un-coated large-pore MSN (*l*-MSN). These inorganic/organic composite nanomaterials are shown to be capable of interfacing with RBCs without damaging the cells even at relatively high concentrations, as observed through electron microscopy, UV−vis spectroscopy, and flow cytometry analyses. Interestingly, the absence of cholesterol in the outer bilayer composition is shown to produce toxic effects without resulting in hemolysis. By maintaining the ζ potential of lipid-bilayer-functionalized MSNs similar to that of the hemolytic *l*-MSNs, we demonstrate that the bilayer composition, and not the surface charge, plays a significant role in determining the hemocompatibility of MSN-based materials.

KEYWORDS: lipid bilayer, hemocompatibility, mesoporous silica, electron microscopy, hemolysis
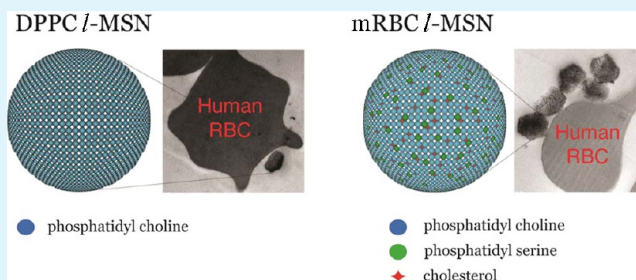
1. INTRODUCTION

During the proceeding decade, research into materials for use as pharmaceutical delivery devices has seen considerable growth. However, questions regarding the toxicity and circulation of these systems have not been fully answered. One of the major issues surrounding the safety and efficacy of such delivery platforms is that of hemocompatibility. A material capable of releasing pharmaceutical compounds on demand is neither safe nor effective if damage occurs among circulating red blood cells (RBCs). The deleterious effects of a RBC-incompatible system could potentially range from bruising at the inoculation site, immunogenic response, and embolism, which can lead to infarction and stroke.[1,2]

The necessity to minimize cytotoxic effects of promising pharmaceutical molecules and increase the efficacy of existing pharmaceuticals has led to the development of many types of drug-delivery devices. Among these, silica-based particles have been extensively researched with regard to their ability to release cargo upon exposure to the correct stimulus, which can include such triggers as pH, light, disulfide reducing agents, enzymes, and magnetic fields.[3−11] While drug release and cell-specific targeting have been demonstrated, there is still a need to fully understand how nanoparticle systems will affect other areas of the body besides the intended target.[12−14] The majority of recent work has been to decrease device fouling caused by nonspecific protein binding and to increase the hemocompatibility of device surfaces by using pendant poly(ethylene glycol) groups.[15−17] However, particles and surfaces that have been prepared to mimic the surface charge or protein composition of the RBC or utilize erythrocyte ghosts to reduce toxicity and increase circulation times have been studied for several decades.[18,19] A powerful strategy for obtaining biocompatible particles is to enclose the particle within a lipid-bilayer structure. Lipid-bilayer-coated particles have been shown to be effective immunoadjuvants and drug-delivery devices and as a platform for biologically active saccharides to bind with cholera toxin.[20,21] Additionally, this method has proven effective in modeling RBCs to study protein insertion and structure via NMR and phagocytosis of healthy and sickle RBCs.[22,23] Future advancements in silica-particle-based therapeutics will require definitive knowledge of in vivo effects, especially hemocompatibility.

With the goal of synthesizing a nanodevice capable of safely interfacing with human RBCs, we investigated the properties of lipid-bilayer-coated large-pore mesoporous silica nanoparticles (LB-*l*-MSNs). Two different outer-leaflet compositions were chosen for particle coatings, the first consisting solely of dipalmitoylphosphatidylcholine (DPPC). The second outer leaflet was composed of a mixture of dipalmitoylphosphatidylserine, DPPC, and cholesterol. Currently, hemotoxicity

reports on silica-nanoparticle systems are limited to morphological effects of the particles and biodistribution.[24−26] Previous reports have shown that MSNs possessing small pores and small, regular particle sizes (e.g., 100−200 nm) are hemocompatible to a concentration of 100 μg mL^{-1}.[25] In contrast, *l*-MSNs ($\approx$800 nm) cause significant hemolysis that could be observed by the naked eye, which was also reported by Hudson et al. with regard to a similar SBA-15 mesoporous silicate.[27] One possible cause of this incompatibility with RBCs has been attributed to interactions between the negatively charged *l*-MSN and zwittionic phosphatidylcholine lipids in the outer RBC membrane (mRBC). As the size of the particle increases, less energy is required to deform the mRBC, allowing for more contact between the RBC and particle. This dual effect of the particle size and surface functionality led to experimental observations that larger silica particles generally show increased hemolytic capability.

Herein, it is shown by flow cytometry examination that there is a high degree of association between MSNs and RBCs. However, transmission electron microscopy evidence indicates that LB-*l*-MSNs are not internalized by RBCs, which is in contrast to the observed behavior of *l*-MSNs in our previous study.[25] Scanning electron microscopy images of cells and particles were obtained in order to further elaborate the results of *l*-MSN/RBC interactions. The standard colorimetric hemolysis assay is used to quantitate the compatibility of nanoparticles with RBCs in many studies.[28] We show, through electron microscopy, that *l*-MSNs can still significantly impact the health of RBCs, while hemolysis data indicate good hemocompatibility. Furthermore, we show that a minimization of the deleterious effects of *l*-MSNs on RBCs can be achieved through a small manipulation in the lipid/cholesterol composition of the outer leaflet of the particle-supported bilayer.

2. EXPERIMENTAL SECTION

2.1. MSN Synthesis. *l*-MSNs were synthesized via our previously reported procedure.[29] The surfactant Pluronic P-104 (7.0 g) as was added to a solution of water (164 g) and 4 M HCl (109 g) and stirred at exactly 55 °C for 1 h in a sealed Erlenmeyer flask. Tetramethyl orthosilicate (TMOS; 10.64 g) was then added at once, and the mixture was stirred for an additional 24 h at 55 °C. This temperature was carefully maintained to achieve the most spherical, uniform particles. The mixture was then added to a Teflon-lined autoclave and treated at 105 °C for 24 h. The product was isolated via filtration, washed sequentially with water and methanol, and lyophilized overnight before further modification. Surfactant was removed via calcination; the *l*-MSN was placed inside a furnace, slowly ramped (1.5 °C min^{-1}) to 550 °C, and allowed to stand at that temperature for 4 h. The material is then characterized via powder X-ray diffraction (XRD), electron microscopy, and nitrogen sorption analysis [Brunauer−Emmett−Teller (BET) and Barrett−Joyner−Halenda (BJH) methods]. Particles labeled with fluorescein are prepared by mixing 2 mg of fluorescein isothiocyanate with 7 μL of (3-aminopropyl)-trimethoxysilane in 2 mL of anhydrous acetonitrile or dimethyl sulfoxide and allowed to react for 10 min. The mixture was then directly added to 1.0 g of *l*-MSN, stirring in 50 mL of anhydrous toluene at 115 °C, and allowed to react overnight. The product was collected via filtration, washed with methanol, and lyophilized overnight, resulting in fluorescein-labeled *l*-MSNs (*l*-[f]MSNs).

The lipid-bilayer-functionalized particles are synthesized according to our previously reported method.[30] Particles with surfactant removed (1.0 g) are dried in vacuo overnight at 110−115 °C; the flask is then backfilled with argon. A solution of anhydrous toluene (50 mL) and 100 mM (mercaptopropyl)trimethoxysilane (MPTMS) is then quickly added to the flask and stirred at 115 °C for 24 h. The product was filtered and washed with copious amounts of methanol to remove any unreacted MPTMS and was then dried in vacuo for approximately 8 h. The product (1.0 g) was then resuspended in 50 mL of anhydrous methanol and 2,2′-dipyridyl disulfide added, and the mixture was stirred overnight. The product was again filtered and washed with copious amounts of methanol and then immediately resuspended in 50 mL of anhydrous methanol. 1-Thiol-2,3-dipalmitoylpropane (0.540 g) was then added to the flask, and the mixture was allowed to stir for an additional 24 h. The product was filtered, washed with methanol, and lyophilized overnight, resulting in a highly hydrophobic dipalmitoyl-functionalized *l*-MSN (DP-*l*-MSN). This hydrophobic *l*-MSN was then placed in a solution containing 1 mg mL^{-1} of the desired bilayer constituents in chloroform. In this study, we examined the effects of a simple DPPC bilayer and one that more closely mimics the surface of the RBC. The mimic layer composition was 40% DPPC, 10% dipalmitoylphosphatidylethanolamine, and 50% cholesterol by weight (mRBC).[31,32] During a typical synthesis, 10 mg of DP-*l*-MSN was placed in a 20 mL glass scintillation vial and a chloroform/outer layer solution added so that there was a total of 3 mg of membrane constituent; chloroform was then added to a total of 10 mL. The mixture was then sonicated for several seconds and allowed to stand approximately 30 min with intermittent shaking. Chloroform was then removed via rotary evaporation, and 10 mL of a pH 7.4 phosphate buffer (no NaCl, 15 mM P$_i$) was added. The mixture was sonicated again for several seconds to detach the particles from the wall of the vial and then allowed to stand another 30 min with intermittent shaking. Mixtures were transferred to glass centrifuge tubes and spun at 345g for 10 min. The phosphate buffer was decanted, an additional 10 mL of buffer was added, and the particles are then resuspended with mechanical shaking and centrifuged a second time. After the second decantation of the buffer, the particles are ready to be used in further experiments.

2.2. MSN Characterization. The particles were characterized by XRD in a Rigaku Ultima IV diffractometer, nitrogen sorption analyses on a Micromeritics Tristar 3000 surface area and porosity analyzer using the BET equation to calculate the apparent surface area and pore volume and the BJH method to calculate the pore-size distribution, thermogravimetric analysis (TGA) in a TGA 2950 thermogravimetric analyzer with a temperature ramp rate of 5 °C min^{-1} in air, dynamic light scattering size analyses of particle suspensions in a Malvern Nano HT Zetasizer, scanning electron microscopy (SEM) of samples coated with iridium in a FEI Quanta 250 FEG microscope, and transmission electron microscopy (TEM) of samples supported on carbon grids in a Tecnai G2 F20 microscope operated at 200 kV.

2.3. Blood Collection and Handling. Approximately 4 mL of a human blood sample, taken from healthy volunteers (ethylenediaminetetraacetic acid stabilized), was freshly collected from the Occupational Medicine office, Ames Laboratory, and was centrifuged at 345g for 5 min. The plasma and buffer-coated layers were removed, and the remaining RBCs were washed with sterile isotonic phosphate-buffered saline (PBS). After the RBCs were washed five times with PBS, no traces of plasma were observed in the supernatant solution. The packed RBCs were used for all of the experiments.

2.4. Flow Cytometry. For labeling with PKH26 (red fluorescent cell linker kit, Sigma, USA), 100 μL of packed RBCs was suspended in 1 mL of diluent C and then mixed with 1 mL of diluent C containing 4 μM PKH26 followed by incubation at room temperature in the dark for 5 min. The reaction was terminated by adding 1 mL of plasma (heat inactivated at 57 °C in an oil bath for 1 h beforehand). The stained RBCs were then centrifuged at 345g for 5 min followed by six washing cycles with PBS to remove the excess and free PKH26 dye. The labeled RBCs were used for flow cytometry analysis.

2.5. Hemolysis Assay. For hemolysis experiments, 200 μL of packed RBCs was diluted to 4 mL with PBS (5% hematocrit), and the diluted RBC suspension (0.2 mL) was mixed with 0.8 mL of *l*-MSN suspensions in PBS at 25, 50, and 100 μg mL^{-1} concentration. Water and PBS (0.8 mL) incubated with 0.2 mL of a diluted RBC suspension served as positive and negative controls, respectively. All of the mixtures were gently vortexed and incubated at room temperature for 2 h. The mixtures were then centrifuged at 345g for 5 min. The

supernatant was transferred to a cuvette, and the absorbance was measured at 541 nm by an Agilent UV–vis spectrometer. The following formula was used to calculate the percent hemolysis of RBCs:

$$\text{hemolysis \%} = \frac{\text{sample abs.} - \text{negative control abs.}}{\text{positive control abs.} - \text{negative control abs.}} \times 100$$

Both the flow cytometry and hemolysis measurements were recorded in triplicate to ensure accuracy and precision in our experimentation.

2.6. Cell Fixing and Electron Microscopy. The diluted RBC suspension (0.2 mL) was mixed with 0.8 mL of l-MSN suspensions in PBS at 25, 50, and 100 μg mL^{-1} concentrations and incubated at room temperature for 2 h. The samples were then fixed by adding a 1% glutaraldehyde solution in PBS dropwise over 5 min and further incubated at 37 °C for 1.5 h, followed by postfixation with 2% osmium tetroxide in PBS for 1.5 h. The RBCs were then dehydrated in increasing concentrations of ethanol (50, 60, 70, 80, 90, 95, and 100%) for 15 min each. Cell suspensions (10 μL) were dropped onto plastic coverslips, dried, and coated with iridium before viewing under a FEI Quanta 250 FEG scanning electron microscope.

The same procedure for preparing samples for SEM imaging was also used for preparing, fixing, and dehydrating the samples followed by staining with 1% uranyl acetate in 70% ethanol at room temperature overnight for TEM. The cells were washed three times with pure acetone and embedded in Epon. The embedded samples were sectioned into 80-nm-thick slices on a Leica Ultracut sliding ultramicrotome. Thin sections were supported on copper grids with a carbon film and examined in a Tecnai G2 F20 microscope operated at 200 kV.

3. RESULTS

3.1. Characterization of MSNs. In this study, two lipid-bilayer compositions (mRBC and DPPC) were tested for hemocompatibility and compared with our previously published data.[25] Physical measurements were obtained including TEM, SEM, XRD, and nitrogen sorption isotherms, confirming an expected semispherical morphology and 2D hexagonal pore structure (Figure 1). ζ-potential measurements of l-MSNs,
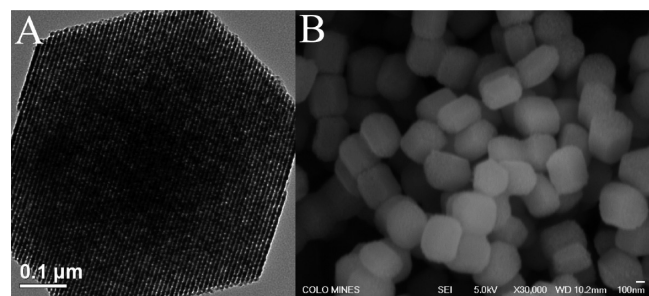

Figure 1. (A) l-MSN particles shown to have a 2D hexagonal arrangement of pores via TEM. (B) SEM images showing that the particles are uniform and have the same approximate radius in all dimensions, rendering them mostly spherical.

DPPC-l-MSNs, and mRBC-l-MSNs reveal that the particles have surface charges of −28.0,[33] −29.8 ± 1.4, and −27.5 ± 1.2 mV, respectively. At physiological pH, silanol groups (p$K_a \approx 4$) on the particle surface are deprotonated, imparting a negative charge to the particle. After the particles have been coated with the lipid bilayer, phosphatidyl moieties from the polar lipid head groups contribute to surface charge because the silanol groups are now masked by the bilayer and by partial replacement of the surface silanols with 3-mercaptopropyl groups by silane grafting.

3.2. Hemolysis. The hemolytic activity of LB-l-MSNs on RBCs was observed using UV–vis measurements (Figure 2) and digital photography (Figure 3). Surprisingly, l-MSNs functionalized with lipid bilayer do not cause any measurable hemolysis above that of the negative control. Visual inspection of the hemolysis experiments shows a clear color differential between samples with small and large amounts of hemolysis. Studies on other particle systems have determined that increasing the positive charge density of the particle leads to a decrease in hemolysis.[34] When acidic silanols on MSNs have been masked by the lipid bilayer, no hemolysis is observed.

3.3. Flow Cytometry. Negligible hemolysis was observed via UV–vis measurements in samples containing LB-l-MSNs, possibly because of low association of particles with RBCs. In order to quantify the amount of particles associated with RBCs, flow cytometry measurements of LB-l-[f]MSNs mixed with PKH26-labeled RBCs were performed. A series of controls were carefully selected to ensure that signals from RBCs associated with LB-l-MSNs do not overlap with signals from unassociated cells. The results of these experiments indicate that particles in solution are closely associated with RBCs (Figure 4). Interestingly, while LB-l-MSNs are observed to produce a unique signal [l-MSN(−) samples], this signal was not observed when particles were mixed with RBCs, indicating that all LB-l-MSNs are associated with RBCs. Because it is possible that the dye-labeling RBCs could become adsorbed by LB-l-MSNs, controls [l-MSN(+)] were established in which LB-l-MSNs were exposed to PKH26. Measurements from flow cytometry show no signals in the gated region for PKH26 and LB-l-MSNs can be observed in the normal region for fluorescein-labeled particles (see the Supporting Information, SI).

Further evidence demonstrating the hemocompatibility of LB-l-MSNs, specifically mRBC-l-MSN, was observed during SEM measurements of fixed RBCs (Figure 5). The series of micrographs in Figure 5 illustrates how changes in the composition of the outer bilayer of MSNs can affect the RBC morphology. In our previous study by Zhao et al.,[25] l-MSNs were shown to be associated with spiculated RBCs under SEM observation. The control population of RBCs (Figure 5A,D) shows only normal discocytes, while RBCs exposed to DPPC-l-MSNs show a large proportion of spiculated cells of echinocyte phases II and III associated with the particles (red circles; Figure 5B,E).[35] A smaller proportion of RBCs, which do not appear to be damaged, can be observed with particles on their surfaces (green circles). When the composition of the particle lipid bilayer was changed to mRBC, the majority of cells observed appear as normal discocytes and spiculation of cells appeared to proceed no further then echinocyte phase I (Figure 5C,F).

During the course of our previous study, TEM observations showed that l-MSNs were enveloped by the mRBC.[25] While there are several systems that utilize the interior of the RBC to deliver cargo, this was not the intended purpose of the LB-l-MSN drug-delivery system. Instead, by using mRBC coatings, we aim to avoid detrimental deformation of RBCs. TEM images of LB-l-MSNs show markedly less local deformation than unfunctionalized (uncoated) l-MSNs (Figures 6 and 7). Similar to SEM observations, mRBC-l-MSNs in contact with RBCs do not appear to cause spiculation and DPPC-l-MSNs appear to be in contact with spiculated RBCs. A study of the hemocompatibility of hydroxyapatite nanoparticles shows
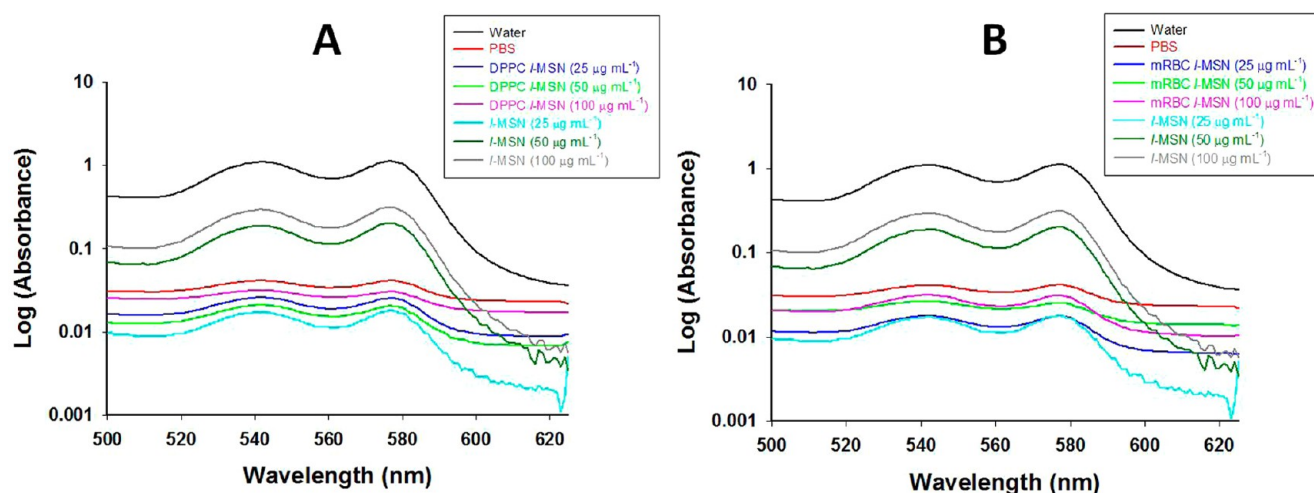
Figure 2. UV−vis spectra of tests for the hemolytic activity of LB-*l*-MSNs. Spectra have been plotted on a log *y* axis for better visualization of the traces. Uncoated *l*-MSNs show high hemolytic activity, roughly 40% of the positive hemolysis control of RBCs in water. In contrast, both LB-*l*-MSNs in parts A (DPPC) and B (mRBC) show hemolytic activity near or below that of the negative hemolysis control, RBCs in a PBS buffer. The baselines of *l*-MSNs are shifted because of scattering of the yellow-red wavelengths by particles. The discrepancies in the baselines for solutions containing particles result from the aggregation of particles and adsorption of yellow to red light by particles and their aggregates that could not be removed through centrifugation.
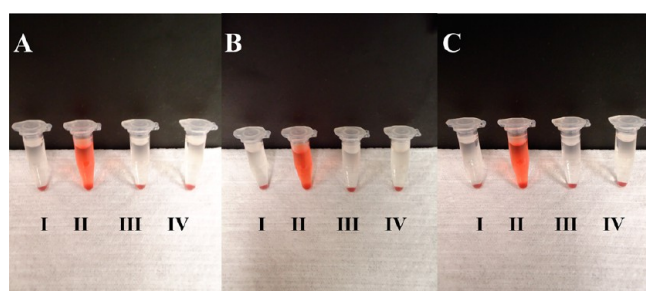

Figure 3. Photographs of the results of hemolysis assays in Figure 2. Labels I−IV correspond to human RBCs under the following conditions: PBS, water, PBS with DPPC-*l*-MSN, and PBS with mRBC-*l*-MSN, respectively. Panels A−C correspond to experiments with differing concentrations of MSN (25, 50, and 100 μg mL^{-1} of particles, respectively). Only the positive hemolysis control sample showed any significant visible hemolysis.

similar results, wherein there is no significant hemolysis, yet TEM images show deformation of the mRBC.[36]

4. DISCUSSION

Because the ζ potentials of the unfunctionalized and lipid-bilayer-coated MSNs are approximately equivalent, these findings would suggest that the hemotoxicity of *l*-MSNs cannot be attributed only to the surface charge. Hemolysis experiments and electron micrographs show that lipid-bilayer-coated *l*-MSNs are much more hemocompatible than bare *l*-MSNs with similar size and ζ potential. The addition of electron microscopy images to the traditional hemolysis studies provides a very important piece of secondary information: that simple RBC lysis cannot and should not be the only indicator of hemocompatibility, at least in studies of mesoporous silica particles. Electron micrographs (both TEM and SEM) of particle/RBC interactions involving DPPC-*l*-MSNs clearly show damage to RBCs in the form of spiculated cells, while *l*-MSNs coated with lipids and cholesterols in proportion to what is found in the RBC outer leaflet show very little in the way of spiculation.
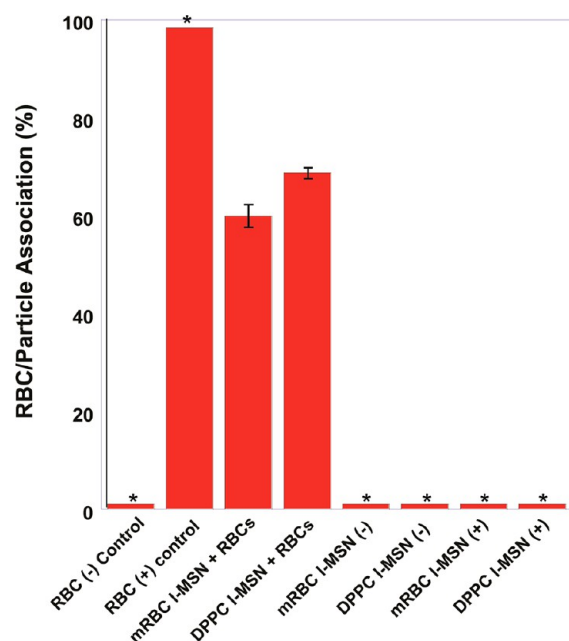

Figure 4. Results of flow cytometry measurements. RBC(−) and (+) controls confirm positive labeling by the PKH26 marker. Samples mRBC- and DPPC-*l*-MSNs were evaluated based on the number of RBCs that were observed to also be positive for fluorescein fluorescent signals. mRBC- and DPPC-*l*-MSN(−) and (+) controls show that fluorescein-labeled particles do not exhibit any fluorescent signals in the region expected for PKH26. Error bars show the percent standard deviation for three samples, and samples marked with asterisks show less than 0.1% standard deviation.

Hemolysis studies performed on the particles in this study demonstrate that coating the particles with lipid bilayers drastically reduces the occurrence of RBC lysis compared to unfunctionalized particles. Particles lacking a lipid coating may cause hemolysis because of the attraction between the negative surface charges of the particle and the positively charged choline lipids that make up the majority of the outer mRBC.
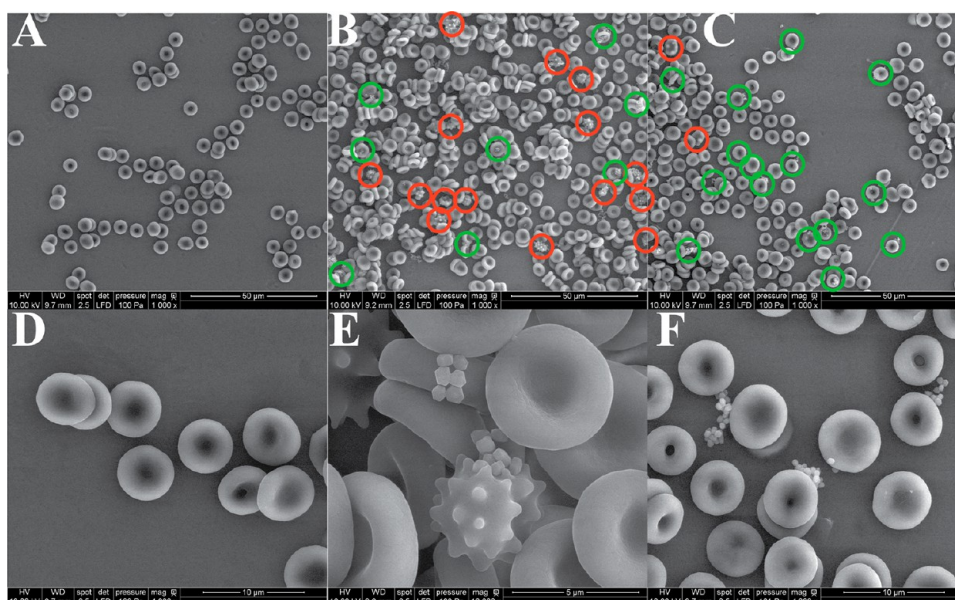
Figure 5. SEM micrographs of RBCs. Cells in panels A and D are control populations not exposed to MSNs. RBCs in panels B and E are exposed to concentrations of DPPC-*l*-MSNs at 50 μg mL^{-1}, and cells associated with particles show a large amount of damage in the form of spicules. Panels C and F show RBCs exposed to concentrations of mRBC-*l*-MSNs at 50 μg mL^{-1}. RBCs in these images appear largely undamaged even when clearly associated with particles. Additional SEM images and the healthy/unhealthy counting method can be found in the SI.
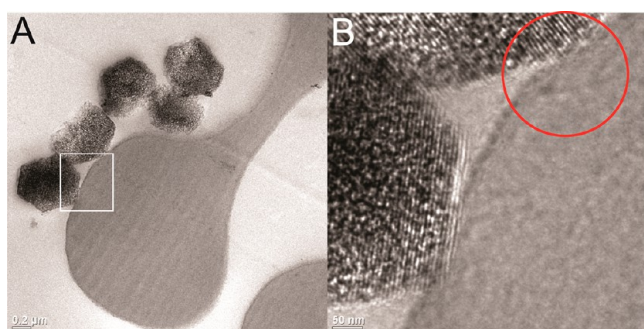

Figure 6. *l*-MSNs coated with phospholipids, which roughly approximate the mRBC. MSNs are shown to be in contact with the RBC membrane; however, significant deformation of the RBC membrane, spiculation of the cell, and endocytosis of the particle is not observed. The right panel (B) shows a magnified image of the area marked by the white box in panel A. Notice that while there is a slight curvature to the RBC membrane in the area of the red circle, the overall cell morphology still resembles that of a healthy cell.
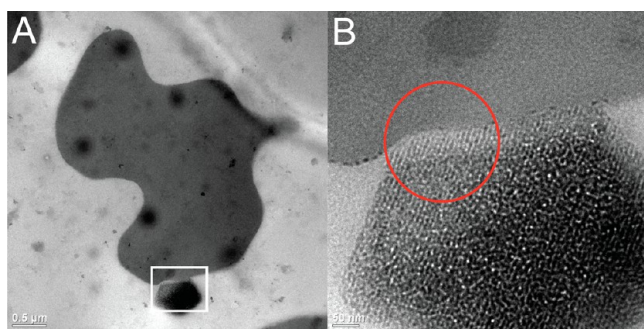

Figure 7. *l*-MSNs coated with only DPPC. MSN is shown to be in contact with a spiculated cell. A clear bending of the RBC membrane is also observed at the corner of the particle (highlighted). The right panel (B) shows a magnified image of the area marked by the white box in panel A. Notice the marked curvature of the RBC membrane.

The ion interaction provides enough energy to cause a deformation of the RBC membrane, which results in spiculation or hemolysis of RBCs and sometimes internalization of the particle.[25] Additional studies have also shown that RBCs in acidic environments are more prone to crenation, which can then lead to the generation of spicules.[37,38] Acidic silanol groups on the surface of MSN may potentially create acidic microenvironments upon association with the RBC membrane, promoting membrane deformation and eventually spiculation.

While initial hemolysis and flow cytometry data showed good hemocompatibility of DPPC-*l*-MSNs, the large amount of damaged cells observed in the SEM micrographs indicated that the DPPC coating may have adverse affects on the ability of RBCs to deform when passing through capillaries, leading to possible clots and necrosis in living systems. There is also evidence in recent toxicological studies that shows a sharp increase in the silicon concentration of the spleen and liver shortly after the administration of MSNs, especially when the dose is given intravenously.[24,39] The close association of MSNs and RBCs observed with flow cytometry coupled with a sharp increase in the silicon concentrations of the spleen might indicate that RBCs undergo spiculation and are removed from circulation in the spleen by a normal biological process.[40] In contrast to DPPC-*l*-MSNs, particles coated with a mRBC do not appear to cause spiculation of RBCs by SEM analysis. Several recent reports also show that a change in the composition of liposomes yields materials with different hemocompatibilities.[41−44] Many of the changes in the hemolytic activity of these materials is generally small, on the order of several percent of the positive control for hemolysis or less.[45] This evidence coupled with the lack of hemolysis and close association of particles and RBCs indicates that mRBC-coated particles may be better candidates as drug-delivery devices because of an improved biocompatible coating. Alternatively, the DPPC-*l*-MSNs may be regaining some ability to damage RBCs through shedding of the outer lipid layer. Cholesterol has long been shown to provide stability to lipid

bilayers and unilamellar vesicles. Recently, more studies have been published that strive to model the liquid crystalline structure of cholesterol/lipid architectures.[46−48] These structures are less likely to dissolve into the surrounding media and therefore represent better coatings for solid particles than formulations lacking cholesterol.

5. CONCLUSION

We have successfully demonstrated that when the outer leaflet of lipid-bilayer-enveloped *l*-MSN is altered, it is possible to prevent damage to RBCs caused by the particles. While hemolysis quantification has been used to determine the hemocompatibility of particles and drugs in the past, this study clearly shows that this is not the only indicator of RBC health. By altering the outer leaflet of the lipid-bilayer-coated *l*-MSNs, we are able to significantly reduce spiculation damage to RBCs. Together these data demonstrate that mRBC-*l*-MSNs represent a positive step toward the formulation of injectable mesoporous silicas for drug delivery and other biological applications.

■ ASSOCIATED CONTENT

ⓢ Supporting Information

Raw data from flow cytometry regarding RBC association with *l*-MSNs and additional SEM images and a counting method for healthy/damaged RBCs along with additional material characterization data. This material is available free of charge via the Internet at http://pubs.acs.org.

■ AUTHOR INFORMATION

Corresponding Author

*E-mail: btrewyn@mines.edu.

Present Address

†B.G.T.: Department of Chemistry and Geochemistry, Colorado School of Mines, Golden, CO 80401.

Author Contributions

The manuscript was written through contributions of all authors. All authors have given approval to the final version of the manuscript.

Notes

The authors declare no competing financial interest.

■ ACKNOWLEDGMENTS

■ REFERENCES

(1) Caplan, L. R.; Hennerici, M. *Arch. Neurol. (Chicago)* **1998**, *55*, 1475.

(2) Li, S.-D.; Huang, L. *Mol. Pharm.* **2008**, *5*, 496.

(3) Gan, Q.; Lu, X.; Yuan, Y.; Qian, J.; Zhou, H.; Lu, X.; Shi, J.; Liu, C. *Biomaterials* **2011**, *32*, 1932.

(4) Lee, C.-H.; Cheng, S.-H.; Huang, I. P.; Souris, J. S.; Yang, C.-S.; Mou, C.-Y.; Lo, L.-W. *Angew. Chem., Int. Ed.* **2010**, *49*, 8214.

(5) Febvay, S.; Marini, D. M.; Belcher, A. M.; Clapham, D. E. *Nano Lett.* **2010**, *10*, 2211.

(6) Vivero-Escoto, J. L.; Slowing, I. I.; Wu, C.-W.; Lin, V. S. Y. *J. Am. Chem. Soc.* **2009**, *131*, 3462.

(7) Bernardos, A.; Mondragon, L.; Aznar, E.; Marcos, M. D.; Martinez-Manez, R.; Sancenon, F.; Soto, J.; Barat, J. M.; Perez-Paya, E.; Guillem, C.; Amoros, P. *ACS Nano* **2010**, *4*, 6353.

(8) Patel, K.; Angelos, S.; Dichtel, W. R.; Coskun, A.; Yang, Y.-W.; Zink, J. I.; Stoddart, J. F. *J. Am. Chem. Soc.* **2008**, *130*, 2382.

(9) Lai, C.-Y.; Trewyn, B. G.; Jeftinija, D. M.; Jeftinija, K.; Xu, S.; Jeftinija, S.; Lin, V. S.-Y. *J. Am. Chem. Soc.* **2003**, *125*, 4451.

(10) Luo, Z.; Cai, K.; Hu, Y.; Zhao, L.; Liu, P.; Duan, L.; Yang, W. *Angew. Chem., Int. Ed.* **2011**, *50*, 640.

(11) Varadan, V. K.; Chen, L.; Xie, J. *Nanomedicine: Design and applications for Magnetic Nanomaterials, Nanosensors and Nanosystems*; John Wiley & Sons, Ltd.: West Sussex, U.K., 2009.

(12) Cheng, K.; Blumen, S. R.; MacPherson, M. B.; Steinbacher, J. L.; Mossman, B. T.; Landry, C. C. *ACS Appl. Mater. Interfaces* **2010**, *2*, 2489.

(13) Brevet, D.; Gary-Bobo, M.; Raehm, L.; Richeter, S.; Hocine, O.; Amro, K.; Loock, B.; Couleaud, P.; Frochot, C.; Morere, A.; Maillard, P.; Garcia, M.; Durand, J.-O. *Chem. Commun. (Cambridge, U.K.)* **2009**, 1475.

(14) Fisichella, M.; Dabboue, H.; Bhattacharyya, S.; Lelong, G.; Saboungi, M.-L.; Warmont, F.; Midoux, P.; Pichon, C.; Guerin, M.; Hevor, T.; Salvetat, J.-P. *J. Nanosci. Nanotechnol.* **2010**, *10*, 2314.

(15) Guo, Z.; Meng, S.; Zhong, W.; Du, Q.; Chou, L. L. *Appl. Surf. Sci.* **2009**, *255*, 6771.

(16) Gulati, N.; Rastogi, R.; Dinda, A. K.; Saxena, R.; Koul, V. *Colloids Surf., B* **2010**, *79*, 164.

(17) Meyers, S. R.; Grinstaff, M. W. *Chem. Rev.* **2011**.

(18) Gaudreault, R. C.; Bellemare, B.; Lacroix, J. *Anticancer Res.* **1989**, *9*, 1201.

(19) Hamidi, M.; Zarrin, A.; Foroozesh, M.; Mohammadi-Samani, S. *J. Controlled Release* **2007**, *118*, 145.

(20) Carmona-Riveiro, A. M. *Int. J. Nanomed.* **2010**, *5*, 249.

(21) Moura, S.; Carmona-Ribeiro, A. *Cell Biochem. Biophys.* **2006**, *44*, 446.

(22) Mani, R.; Cady, S. D.; Tang, M.; Waring, A. J.; Lehrer, R. I.; Hong, M. *Proc. Natl. Acad. Sci. U. S. A.* **2006**, *103*, 16242.

(23) Symes, M. A.; Patel, H. M. *Biochem. Soc. Trans.* **1992**, *20*, 327S.

(24) Huang, X.; Li, L.; Liu, T.; Hao, N.; Liu, H.; Chen, D.; Tang, F. *ACS Nano* **2011**, *5*, 5390.

(25) Zhao, Y.; Sun, X.; Zhang, G.; Trewyn, B. G.; Slowing, I. I.; Lin, V. S.-Y. *ACS Nano* **2011**, *5*, 1366.

(26) Joglekar, M.; Roggers, R. A.; Zhao, Y.; Trewyn, B. G. *RSC Adv.* **2013**, *3*, 2454.

(27) Hudson, S. P.; Padera, R. F.; Langer, R.; Kohane, D. S. *Biomaterials* **2008**, *29*, 4045.

(28) ASTM Protocol E2524-08. *Standard Test Method for Analysis of Hemolytic Properties of Nanoparticles*; ASTM International: West Conshohocken, PA, 2013; DOI: 10.1520/E2524, http://www.astm.org.

(29) Kim, T.-W.; Slowing, I. I.; Chung, P.-W.; Lin, V. S.-Y. *ACS Nano* **2010**, *5*, 360.

(30) Roggers, R. A.; Lin, V. S. Y.; Trewyn, B. G. *Mol. Pharm.* **2012**, *9*, 2770.

(31) Mohandas, N.; Gallagher, P. G. *Blood* **2008**, *112*, 3939.

(32) Narla, M. Red Blood Cell Membrane Dynamics and Organization. *UpToDate online* [Online Early Access]. Published Online: 2010.

(33) Martin-Ortigosa, S.; Valenstein, J. S.; Sun, W.; Moeller, L.; Fang, N.; Trewyn, B. G.; Lin, V. S.-Y.; Wang, K. *Small* **2012**, *8*, 413.

(34) Shelma, R.; Sharma, C. P. *Colloids Surf., B* **2011**, *84*, 561.

(35) Lim, H. W. G.; Wortis, M.; Mukhopadhyay, R. *Proc. Natl. Acad. Sci. U. S. A.* **2002**, *99*, 16766.

(36) Han, Y.; Wang, X.; Dai, H.; Li, S. *ACS Appl. Mater. Interfaces* **2012**, *4*, 4616.

(37) Sergey, V. R. *Biochim. Biophys. Acta, Biomembr.* **2010**, *1798*, 1767.

(38) Rasia, M.; Bollini, A. *Biochim. Biophys. Acta, Biomembr.* **1998**, *1372*, 198.

(39) Liu, T.; Li, L.; Teng, X.; Huang, X.; Liu, H.; Chen, D.; Ren, J.; He, J.; Tang, F. *Biomaterials* **2011**, *32*, 1657.

(40) Mebius, R. E.; Kraal, G. *Nat. Rev. Immunol.* **2005**, *5*, 606.

(41) Kose, G. T.; Arica, M. Y.; Hasirci, V. *Drug Delivery* **1998**, *5*, 257.

(42) Tsuchida, E.; Sakai, H. *Microspheres, Microcapsules Liposomes* **1999**, *2*, 503.

(43) Tagami, T.; Ernsting, M. J.; Li, S.-D. *J. Controlled Release* **2011**, *154*, 290.

(44) Koromila, G.; Michanetzis, G. P. A.; Missirlis, Y. F.; Antimisiaris, S. G. *Biomaterials* **2006**, *27*, 2525.

(45) Kuznetsova, N. R.; Sevrin, C.; Lespineux, D.; Bovin, N. V.; Vodovozova, E. L.; Meszaros, T.; Szebeni, J.; Grandfils, C. *J. Controlled Release* **2012**, *160*, 394.

(46) Suga, K.; Umakoshi, H. *Langmuir* **2013**, *29*, 4830.

(47) Anderson, N. A.; Richter, L. J.; Stephenson, J. C.; Briggman, K. A. *J. Am. Chem. Soc.* **2007**, *129*, 2094.

(48) Khelashvili, G.; Harries, D. *J. Phys. Chem. B* **2013**, *117*, 2411.

1681

dx.doi.org/10.1021/am4045713 | *ACS Appl. Mater. Interfaces* 2014, 6, 1675−1681